The effect of external compressive loads on the cycle lifetime of Lithium-ion pouch cells

Anup Barai[1, *], Ravichandra Tangirala[1], Kotub Uddin[1], Julie Chevalier[2], Yue Guo[1], Andrew McGordon[1], Paul Jennings[1]

[1] WMG, University of Warwick, Coventry, CV4 7AL, United Kingdom

[2] Hybrids and Electrification, Jaguar and Land Rover, Banbury Road, Warwick, CV35 0XJ, United Kingdom

Keywords

Lithium-ion battery; external pressure; capacity fade; power fade; cell ageing; cycle life

Abstract

In application, lithium-ion pouch-format cells undergo expansion during cycling. To prevent contact loss between battery pack components and delamination and deformation during battery operation, compressive pressure is applied to cells in automotive battery modules/packs by way of rigid cell housing within the modules. In this paper, the impact of such compressive pressure on battery degradation is studied. Samples of commercial, 15 Ah $LiNiMnCoO_2$ /Graphite electrode pouch-type cells were cycled 1200 times under atmospheric, 5psi and 15 psi compressive loads. After 1200 cycles, the capacity fade for 0, 5 and 15psi loads was11.0 %, 8.8 % and 8.4 %, respectively; the corresponding power fade was found to be 7.5 %, 39 % and 18 %, respectively, indicating power fade peaks between 0 and 15psi. This contrasting behaviour is related to the wettability increase and separator creep within the cell after compressive load is applied. The opposing capacity fade and power fade results require consideration from automotive battery engineers at the design stage of modules and packs. In addition to capacity fade and power fade results, the study identified the evolution of compressive pressures over multiple cycles, showing that pressure increases with cycling.

1. Introduction

Lithium-ion (Li-ion) batteries provide an attractive alternative to other battery chemistries in part due to high energy storage density, power delivery density and competitive cost. This has resulted in Li-ion batteries being the preferred solution in electric vehicle (EV) applications. In order to exploit the advantage of Li-ion batteries' high energy and power density, in the design and assembly of battery packs for EVs, cells are compactly packaged. Pouch-format cells undergo expansion during cycling by 6 % from rest conditions in the direction normal to the electrode stack [1]. Rigid constraints are applied to the battery pack to maintain packaging compactness, maintain contact between battery components, provide good thermal contact and prevent delamination and deformation during battery operation. A coupling of compact packaging and rigid constraints of Li-ion batteries, at pack level, gives rise to safety issues due to potential overheating of the battery system [2]. The majority of the literature to-date has thus been devoted to understanding the thermal implications of such compact packaging arrangements.

It is well known that under automotive power-draw conditions at ambient operating temperatures, the temperature rise within most Li-ion cells can be significant [3]. Defects in individual cells [4] can further compound the problem by increasing local heat generation [5]. This may lead to thermal runaway of some cells and subsequently the propagation of excessive temperature throughout a module or pack [6]. Much of the literature has therefore focused on 3D thermal modelling of battery packs [2, 7-10] and designing thermal management systems [11-14] to address concerns relating to battery pack safety due to significant self-heating.

The mechanical implication of compact, rigid packaging of lithium ion batteries, on the other hand, has seldom been addressed in the literature. Given the lateral expansion of pouch cells during operation [1] and the rigid housings in which pouch cells that make-up battery modules are placed, each pouch cell in a module/pack ensemble will be subjected to dynamic and compressive pressure which varies over the lifetime of the cell [1]. This issue is more pronounced for cell chemistries which employ electrode materials with higher volumetric expansions such as silicon [15].

Previous studies of in-operando mechanical stress within lithium-ion batteries focus on modelling stress and strain in electrode particles [16, 17] due to the formation of intercalation

gradients in the solid phase, which is linked to particle fracturing and hence capacity and power fade through the isolation of electrode material, and contact loss, respectively [18, 19]. The evolution of compressive pressure due to volume expansion at the macroscopic (i.e., cell level) scale was experimentally quantified by *Wang et. al.* [20, 21]. They reported, performance degradation due to volume expansion, primarily due to structural change of cathode materials.

The impact of compressive pressure loads on cell capacity degradation was studied by *Cannarella et. al.* [22] and *Peabody et. al.* [23]. *Cannarella et. al.* applied 7.2, 72 and 720 psi on pouch-type lithium ion cells and reported less capacity degradation for the 7.2 psi condition compared to unconstrained condition, even after 1800 cycles. For higher pressure conditions the capacity drop was much higher than the unconstrained condition. *Peabody et. al.* considered pressure of 145 psi to 4351 psi. Both these studies restricted their investigation to loss of capacity. Thus, none of these studies reported any change of impedance with pressure, which may be significant. With increased pressure i.e. compressive loads on li-ion pouch cells, resistance rise may occur due to elastic creep of the separator [24]. Also, with the exception of the 7.2 psi condition, the external compressive loads studied in Refs. [22, 23] are too high to be realised in a practical li-ion battery pack for automotive application.

Although battery ageing has received significant research focus to date, it remains as a key unknown to the original equipment manufacturers (OEM). The mechanisms and physical conditions that lead to accelerated battery degradation are not yet completely understood; the effect of external pressure on battery ageing is one such accelerating factor that is still not understood. The aim of this paper is therefore to measure and quantify any accelerated ageing effects on lithium ion cell performance due to cycling for extended periods under constant pressure, representative of commercial battery packs. The effect of external pressure on impedance rise and capacity drop with cycling is investigated. The experimental setup and procedure adopted in this paper is introduced in Section 2. After presenting the results due to applying pressure and cycling, a discussion of the results is outlined in Section 3. Finally, the key findings are summarised in Section 4.

2. Experimental procedure

Commercially available 15Ah Li-ion pouch cells with graphite (C_6) negative electrode and $LiNiMnCoO_2$ (NMC) positive electrode were used for this experiment. The cells had a

maximum charge voltage of 4.2 V with a minimum discharge voltage of 2.5 V. The manufacturer's recommended maximum 10s current was 7C for both charge and discharge. The dimension of the cell is $18.6 \times 16.5 \times 5.6\ cm$. The cells were characterised and cycled with three different externally applied pressures, namely, 0 psi, 5 psi and 15 psi. These pressures were selected in accordance with the estimated pressure within an automotive battery pack. Two cells were tested at each pressure condition and the temperature was kept constant at 25 °C using a temperature chamber.

To emulate the pressure in an assembled automotive pack, 5 psi and 15 psi external pressure were applied to each cell. To achieve a homogenous pressure distribution, cells were sandwiched between two cast iron plates ($20 \times 20 \times 2.5\ cm$), each weighing 7.35 kg, as shown in Figure 1. The order of the set up includes a plate, pouch cell, pressure sensor pad and another plate on top (see Figure 1 (a)). The required pressure was achieved by tightening the M8 bolts located at each corner of the iron plates. The Tekscan 5210N pressure sensor area is made up of 1936 pressure sensing elements, capable of measuring up to 200 psi. Therefore, any imperfection of pressure on the cell surface were measured and corrected using the M8 bolts on the iron plates; this excluded the dynamic high pressure peaks generated during charge-discharge of the battery. The tabs of the pouch cells were clamped in between a nonconductive polymer surface and gold plated brass blocks with a torque wrench set to 12.5 Nm torque. The battery cycler and EIS equipment were connected using brass blocks. The whole arrangement was placed within a temperature chamber to keep the temperature constant at 25 °C. Similar experimental setups were employed in previous studies using oil based diaphragms [25], metal plates with fixed pressure [22] and by a specialist instrument [23] to apply external pressures on pouch cells and study their performance. Hence, the above-mentioned setup is very much in-line with the existing methods of applying external pressure on the cell. Figure 1 (b) shows a photo of the arrangement.

(a)

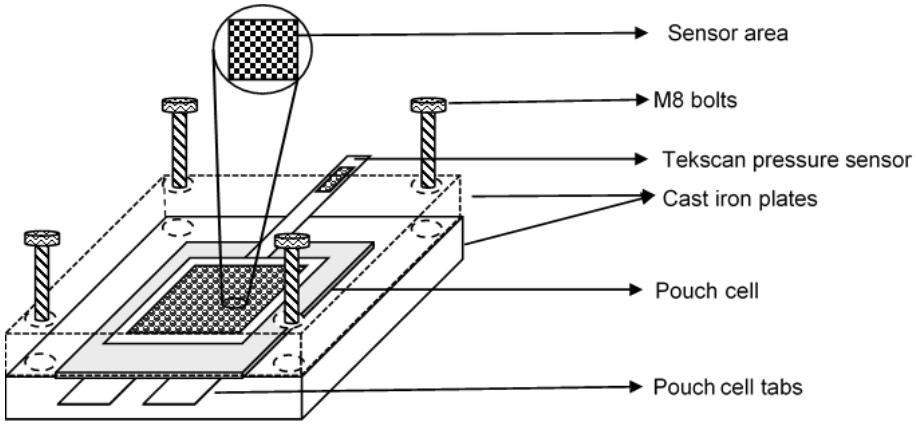

(b)

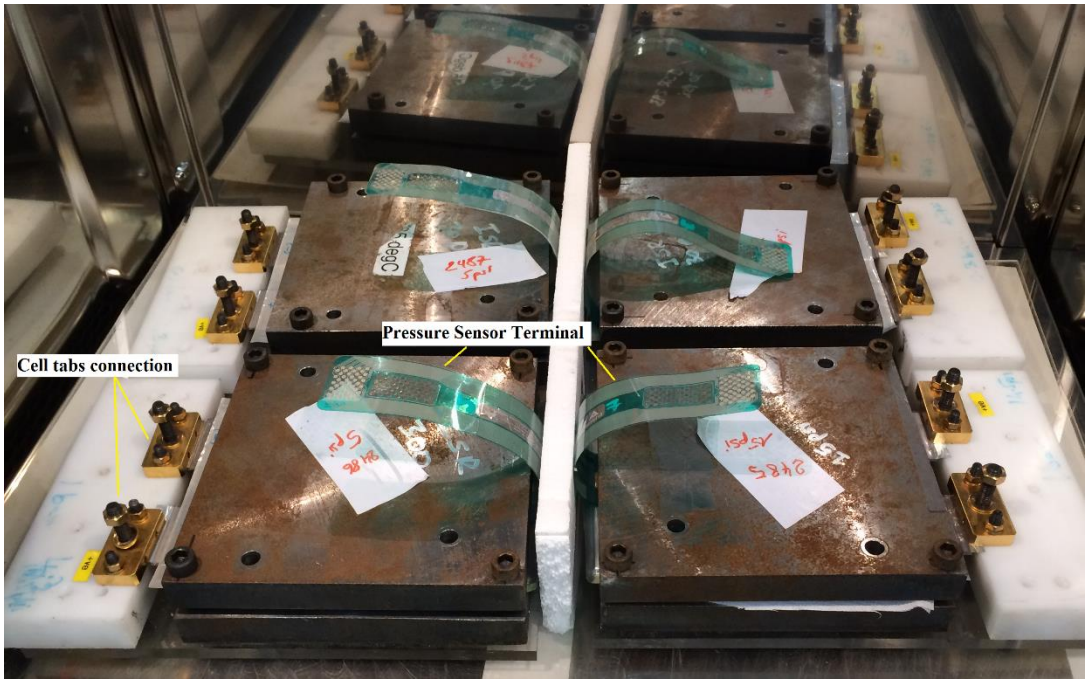

Figure 1: (a) Schematic of the pressure jig arrangement (b) picture showing the pressure jig set-up of the cells and arrangement, (left) 5 psi cells and (right) 15 psi, respectively.

The flowchart of the experimental procedure is shown in Figure 2. To assess the effects of cycling under pressure on the performance degradation of the lithium ion cell, it is necessary to compare the changes in cell performance. Cell performance was characterised using a set of characterization tests, labelled ‘snapshot tests’. A snapshot test comprised of a 1C capacity retention test, pulse power tests and electrochemical impedance spectroscopy (EIS) tests at 90 %, 50 % and 20 % SoC.

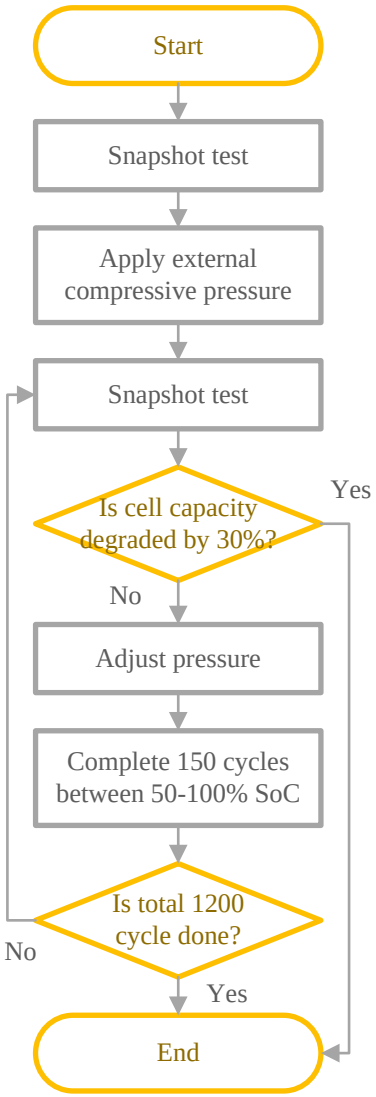

Figure 2: Flowchart of the experimental process.

To determine the 1C capacity, the cells were fully recharged at constant current of 1C up to 4.2 V and then held at 4.2V until the current fell below 0.5 A, using a commercial cell cycler (Bitrode MCV 16-100-5). This was followed by a rest period of 3 h prior to being fully discharged at the 1C rate to the cut-off voltage of 2.5 V. Pulse power tests were performed at 90 %, 50 % and 20 % SoC, using 10 s current pulses of 20 %, 40 %, 60 %, 80 % and 100 % of the cell's rated maximum pulse discharge and charge current. Each pulse at a given current level was followed by a 30 min rest period prior to performing the next pulse. The internal resistance was then calculated from the cell voltage drop due to pulse current.

Electrochemical Impedance Spectroscopy (EIS) measurements were performed after pulse power testing was complete using a Solartron model 2100 fitted with a 2 A booster in

galvanostatic mode using ModuLab® XM ECS software. The EIS spectra collected were in the frequency range of 20 mHz to 20 kHz, with 10 frequency points per decade. The applied amplitude (RMS value) of the signal was set 800 mA, with no DC current being superimposed on the RMS current. The EIS data were recorded 3 h after the last pulse of the pulse power test [26, 27].

Following the first snapshot test, the compressive pressure was applied and another snapshot test was performed to record any change of cell performance due to the compressive pressure. The load pressure was subsequently adjusted before cells were continuously cycled under the applied compressive pressure. This emulated the operation of a cell – within a battery pack – under constant compressive pressure. For cycling, cells were charged from 50 % SoC to 100 % SoC and brought back to 50 % SoC using 1C charge/discharge. Cycling was paused after 150, 300, 450, 600, 800, 950 and 1200 cycles to perform a snapshot test. After every snapshot test, the divergence in surface pressure as a result of ageing was recorded and the M8 bolts were adjusted accordingly so that the desired 5psi and 15psi were maintained. Snapshot and cycling was carried out at 25 ˚C. There were two end conditions set for the test procedure, either the cell capacity degraded by 30 % or 1200 cycles are completed. The 30 % degradation was set to match the end-of-life condition of the commercial automotive battery packs.

3. Results

3.1 Effect of applying external pressure

The pressure map generated by data acquired from the pressure sensing pads for a cell surface under compressive loads is shown in Figure 3. This shows that pressure was evenly distributed for 15 psi. For 5 psi, the pressure was higher around the cell boundaries than in the middle. However, there were no localized high pressure regions across either cell surfaces, which would be identified as a peak on the pressure map. This indicates a uniform surface construction and an absence of gas formation within the cell.

The cell capacity did not change when pressure was applied, however, impedance did change. The capacity value before applying pressure was 15.22 Ah, which was found to be the same when both 5 psi pressure (15.22 Ah) and 15 psi pressure (15.21 Ah) was applied to the cells. The impedance before and after applying pressure is shown in Figure 4. A change of impedance was observed when pressure was applied to the cell. There was a 0.74 mΩ change

of R_o when 5 psi pressure was applied. The corresponding change for 15 psi was 0.58 mΩ. The timescale of Pure Ohmic resistance (R_o), defined to be the point at which the cell changes from inductive to conductive behaviour (i.e., interception of x-axis on the Nyquist plot), was found to be 398 Hz under atmospheric pressure. The onset of external compressive pressure however, changed this to 100 Hz for both pressure conditions. The double layer capacitance (C_{dl}) increased, while charge transfer resistance (R_{ct}) decreased – together contributing to a smaller semicircle in the Nyquist plot. The low frequency, diffusion limited region (Warburg tail) remained unchanged however. These results are in agreement with current understanding [24, 28] which suggests separator creep occurs when pressure is applied. Separator creep reduces ionic conductivity from electrode to electrode, which directly contributes to R_o. In contrast, when pressure is applied, the contact between electrode particles and electrolyte improves (i.e., there is improved wettability) [29] which increases the overall effective double layer area of the cell, contributing to the increase of C_{dl} and decrease of R_{ct}. However, considering that the morphology of electrode particles are not changed (no particle cracking) due to the pressure, the solid-state diffusion contributing to the Warburg tail remains the same. Similar observations can also be made from pulse power test data. Table 1 presents the pulse power test data before and after applying pressure. Due to the limitations of the battery cycling equipment, the voltage drop can only be measured at a resolution of 0.1 secs. Therefore, the resistance measured from a 0.1 sec pulse is not pure Ohmic resistance, but will also contain contributions from charge transfer resistance. Nevertheless, resistance measured after 0.1 sec of a square wave pulse shows a significant change for both external pressure conditions. The change in resistance calculated from longer duration pulses of 1, 2, 5 and 10 secs, show no additional change. This is because although a square-wave pulse gives rise to multiple sine wave harmonics and by extension multiple physical processes/phenomena, only a particular subset of frequencies dominate. That is, in terms of the spectral density, for a 1 sec pulse the maximum power is associated with the 1 Hz harmonics and for a 10 sec pulse, it is 10 Hz. From EIS tests, it can be deduced that the cell enters a diffusion limited Warburg impedance region after 2 Hz, i.e., at frequencies lower than the frequency corresponding to the local minimum in the Nyquist plot (Figure 4). Therefore, pulse timescales of between 0.1 sec and 1sec and longer are in the diffusion limited region, which is not affected by pressure, thus did not shown any change in Table 1.

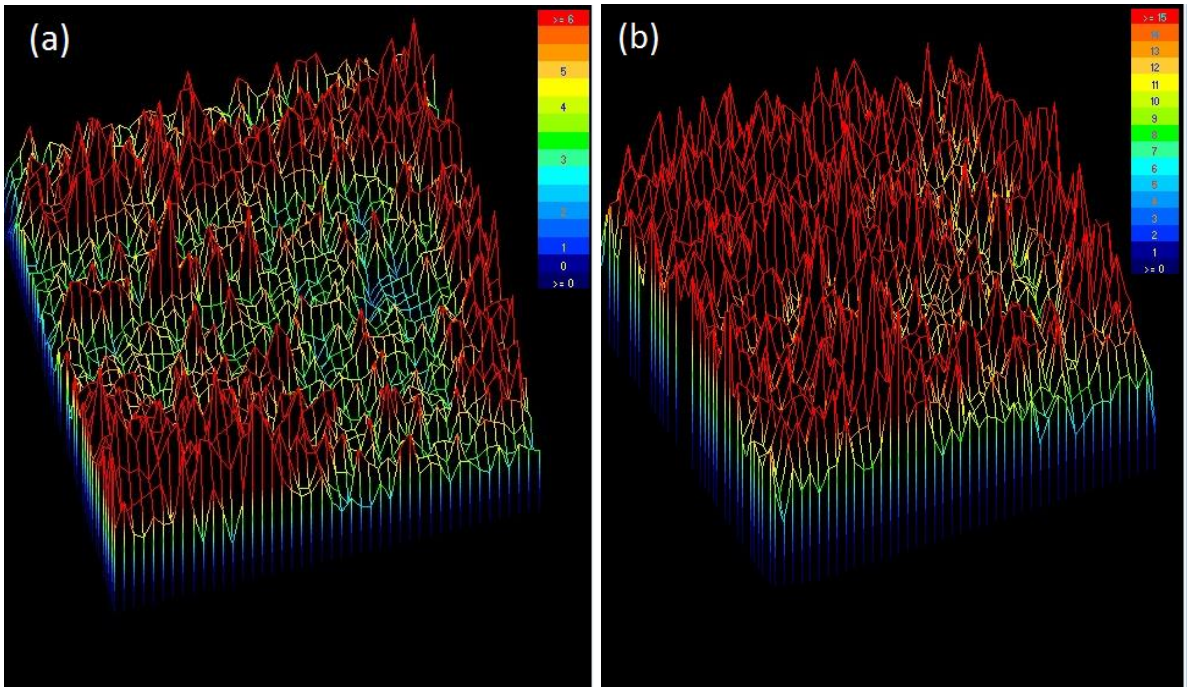

Figure 3: Pressure profile on the cell surface, (a) 5 psi, (b) 15 psi.

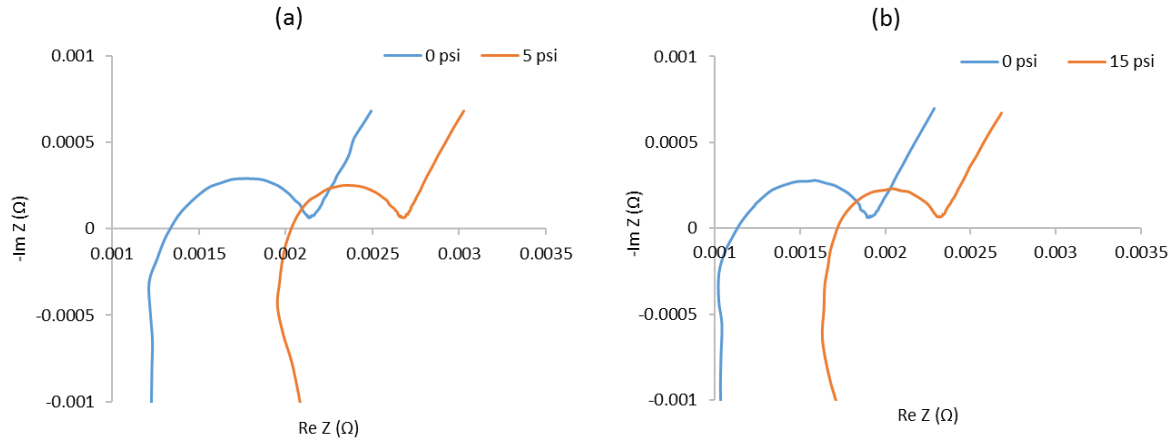

Figure 4: Change of impedance due to external pressure.

Table 1: Change of internal resistance with the application of pressure, measured from pulse power test.

		Resistance (mΩ) from 4 C discharge pulse of difference duration				
		0.1 sec	1 sec	2 sec	5 sec	10 sec
5 psi	Before pressure	2.13	2.33	2.47	2.75	3.12
	After pressure	2.55	2.75	2.87	3.15	3.52
15 psi	Before pressure	1.95	2.17	2.28	2.58	2.95
	After pressure	2.20	2.42	2.53	2.82	3.18

3.2 Effect of cycling ageing

The trend of capacity drop with pressure is presented in Figure 5. The capacity drop trend was identical for all three conditions for the first 450 cycles. After 450 cycles, the cells without any external pressure exhibited higher capacity drop compared to the cells under pressure. After 1200 cycles, the capacity fade was 11.0 % for the cells without any applied external pressure, whereas it was 8.8 % and 8.4 % for 5 psi and 15 psi external pressure conditions respectively.

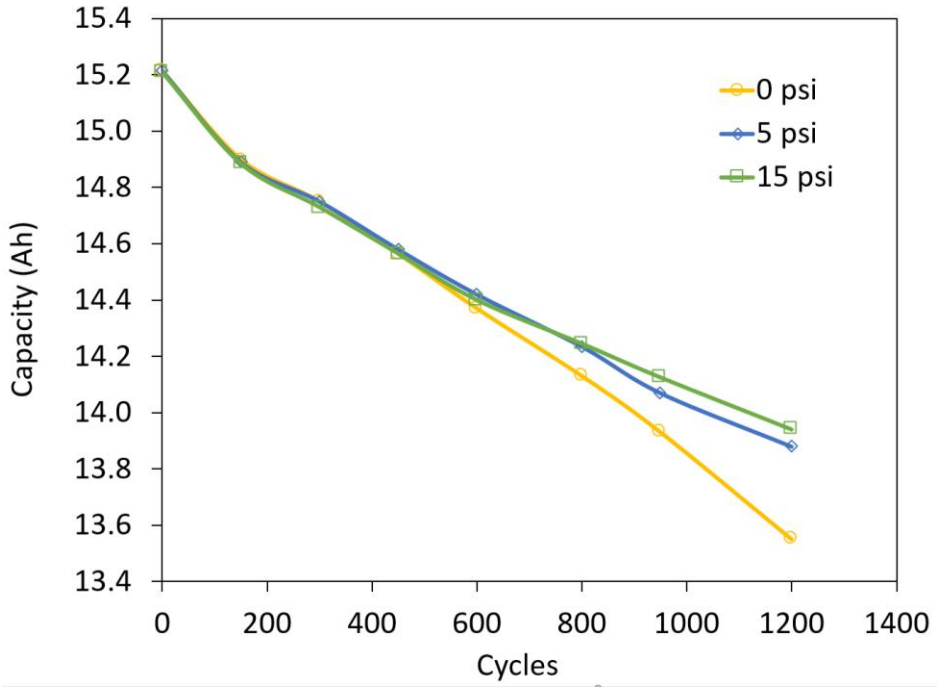

Figure 5: Change of capacity with cycling ageing at different external pressure conditions.

Cell impedance as a function of cycle number and applied pressure is shown in Figure 6, which presents impedance spectroscopy results at 50 % SoC, when the cells were new (but under external pressure), after 600 cycle and after 1200 cycles. Nyquist plots from intermediate snapshots follow the trend shown in Figure 6 but are not presented for clarity. From these results, it is clear that pure Ohmic resistance, R_o, increases in all cases. For cells cycled under atmospheric pressure, R_o increased by 19.6 %, in comparison to 31.7 % and 18.2 % for 5 psi and 15 psi external pressure conditions, respectively. The frequency corresponding to R_o in the Nyquist plots was found to change with cycling and pressure. When the cells were new, R_o was identified to correspond to a 100 Hz, whereas it was found to be 126 Hz, 158 Hz

and 158 Hz after 1200 cycles for 0, 5 and 15 psi conditions respectively. In contrast, double layer capacitance, C_{dl}, and charge transfer resistance, R_{ct}, showed stability over the cycling period, exhibiting negligible change due to cycling. This is attributed to the wettability of the active materials increasing and will be discussed further in Section 3.4.

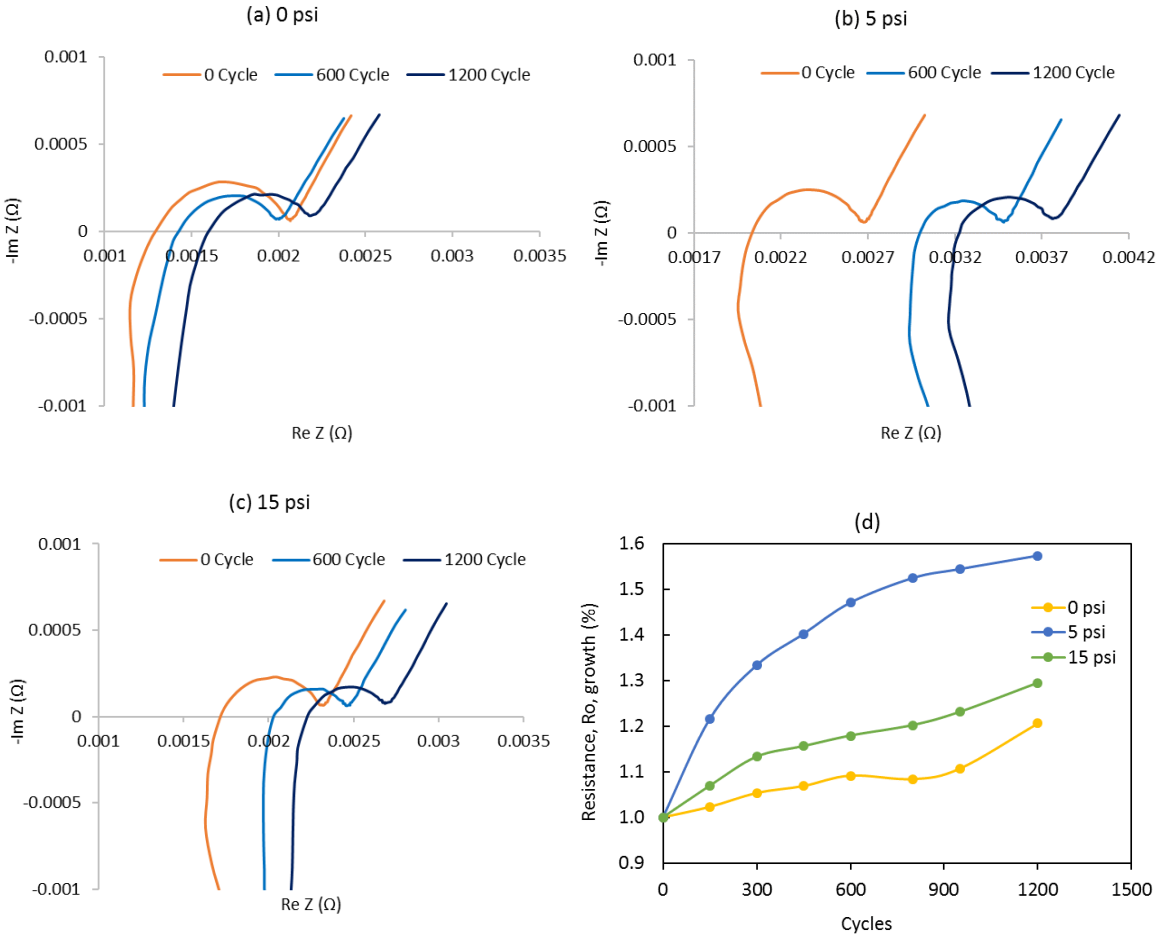

Figure 6: Change of impedance at 50 % SoC due to cycling ageing with 600 and 1200 cycles.

Table 2: Change of internal resistance with cycling measured from pulse power test.

		Resistance (mΩ) from 4 C discharge pulse of difference duration				
		0.1 sec	1 sec	2 sec	5 sec	10 sec
0 psi	0 Cycle	1.98	2.20	2.32	2.60	2.97
	1200 Cycle	2.09	2.37	2.50	2.82	3.20
5 psi	0 Cycle	2.55	2.75	2.87	3.15	3.52
	1200 Cycle	3.59	3.92	4.03	4.33	4.72
15 psi	0 Cycle	2.20	2.42	2.53	2.82	3.18
	1200 Cycle	2.62	2.88	3.02	3.30	3.67

The resistance values calculated from 4 C discharge pulses at 50 % SoC are presented in Table 2. The resistance calculated from the 0.1 sec pulse duration increased by 5.6 % when no compressive pressure was applied, whereas it rose by 40.8 % for the 5 psi condition and 19.1 % for the 15 psi condition. If a 10 sec pulse is considered to be the total resistance rise, as is often done in the literature [19, 30], the total rise in resistance is 7.7 %, 34.1 % and 15.4 % respectively for 0, 5 and 15 psi conditions. Given that the timescale of different physical processes change with cycling (e.g., R_o occurs at different frequencies with pressure and ageing), direct comparison of resistance values from a given pulse length will be limited because the estimated resistance will include contributions from different electrochemical processes.

3.3 Change of pressure with Cycling

During cycling, the compressive pressure felt by a pouch cell changes due to expansion and contraction of host materials due to lithium intercalation. Over multiple cycles, binder swelling [31], viscoelastic creep [23] and irreversible parasitic reaction deposits [32] cause the cell volume to increase. Given the rigidity of the cell housing in battery packs (emulated by the experimental fixture depicted in Figure 1 in this study) the increase in volume leads to an incremental pressure increase as the cell is progressively cycled. The pressure values at the end of every snapshot test are shown in Table 3 and the pressure maps after 150 cycles and 1200 cycles are shown in Figure 7. The pressure is seen to always increase at the end of cycling, with the highest effective compressive pressure changes after 1200 cycles. After the first 150 cycles, pressure increased by 74% for the 5 psi condition and 49% for the 15 psi condition. After 1200 cycles, the pressure increased by 199% for the 5psi condition but remained homogenous. In contrast, the pressure increase was 130% for the 15 psi condition. Unlike previous cases, before performing the last snapshot test at 1200 cycles the cells were cycled for 250 cycles (950 to 1200) which might be the origin of the significant pressure increase observed.

The surface pressure was evenly distributed for 5 psi external pressure condition for the entire test duration, see Figure 7 (a) and (c). In contrast, for the 15 psi condition there were two high pressure points across the surface after first 150 cycles, as shown in Figure 7 (b). The peaks persisted over the entire test duration and were found to increase with cycling (Figure 7 (d)). These peaks may be attributed to inhomogeneity in the active material distribution within the

electrode due to uneven material pasting on the current collectors at the manufacturing stage, which become prominent after the first 150 cycles. Such inhomogeneity would give rise to localised heating and consequently localised peaks in solid electrolyte interphase film formation, therefore, will increase the pressure peaks with cycling.

Table 3: Summarizing the incremental pressure increase of the individual cells after each defined of calendar ageing of 0, 150, 300, 450, 600, 800, 950 and 1200 cycles, respectively.

Cycles	End of cycle pressure for 5 psi condition (psi)	End of cycle pressure for 15 psi condition (psi)
0	5	15
150	8.68	22.32
300	5.80	25.89
450	8.68	21.90
600	6.47	21.07
800	8.63	21.69
950	8.18	21.54
1200	14.94	34.57

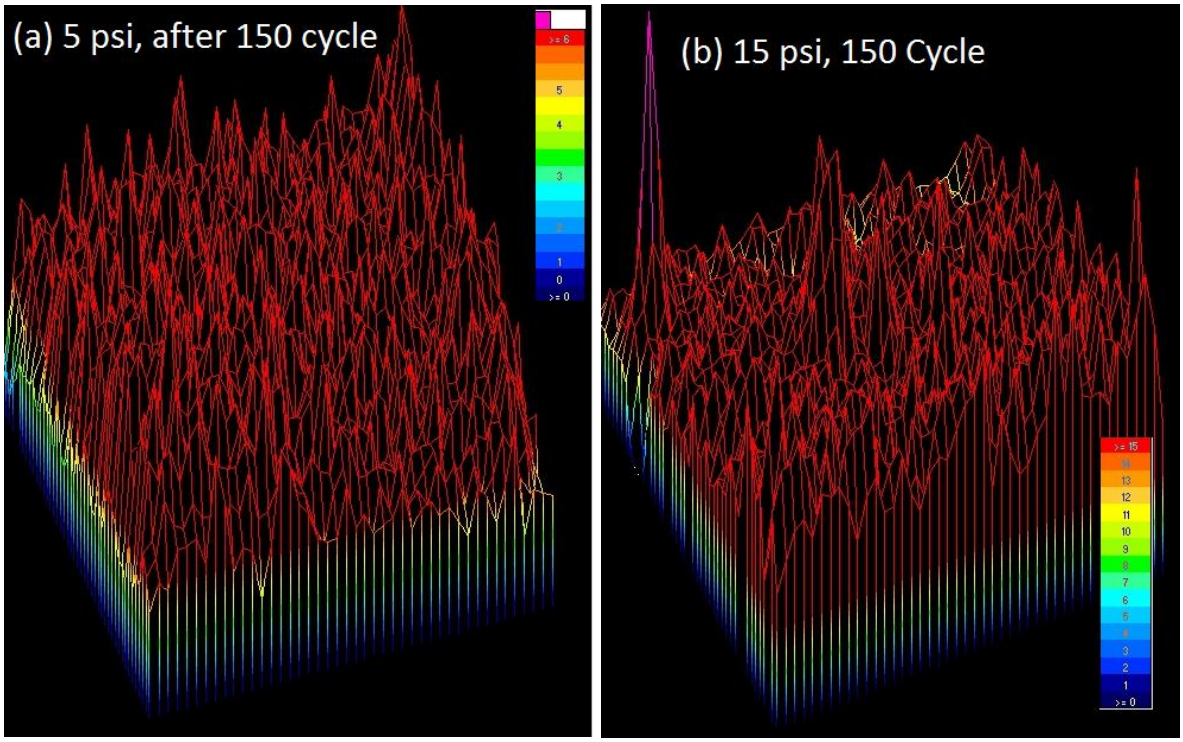

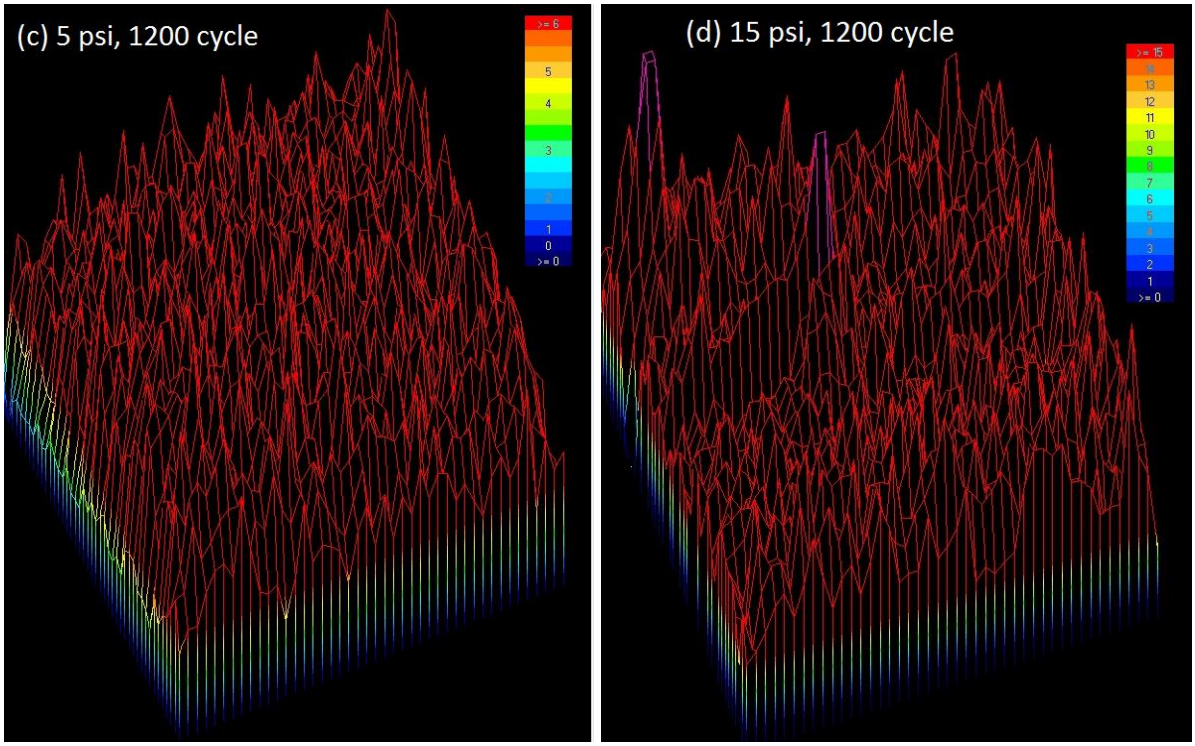

Figure 7: Pressure increase after 150 cycles (a) and (b), and after 1200 cycles (c) and (d).

3.4 Discussion

When an external pressure is applied to a pouch cell, there are primarily two physical mechanisms, separator creep and wettability of the electrodes, which affect the performance of the cell. When pressure is applied, the separator pores creep [24], thus the porosity and tortuosity of the separator changes. With applied pressure, the change of porosity and tortuosity is not linear [24]. The ion transport resistance of the separator is directly related to the porosity and tortuosity following Eq. 1 [33].

$$R = \rho_e \frac{\tau l}{\varepsilon A} \tag{1}$$

where, R is the ion transport resistance through the separator, l is the thickness of the separator, A is the active separator area, ε is the porosity, τ is the tortuosity and ρ_e is the resistivity of the electrolyte.

In contrast, when pressure is applied, the wettability of the electrodes increases; the penetration of the electrolyte into the porous electrodes increases. Increased wettability leads to better contact between electrode materials and electrolyte, i.e., increased double layer which increases the double layer capacitance and reduces ion-transport resistance [29]. These two

mechanisms along with SEI growth due to cycling mainly dominate the degradation of cell performance reported in this study.

3.4.1 Capacity fade with cycling at different pressure

The 1C capacity test results are in agreement with results published by *Cannarella et. al.* [22]. In their work, *Cannarella et. al.* cycled batteries with stack pressures of 7, 72 and 725 psi, and compared the results with no pressure (atmospheric) conditions. They reported higher degradation when 72 and 725 psi pressure was applied, compared to the no additional pressure condition. However, 7 psi showed less degradation than the atmospheric pressure condition. From the post-mortem analysis of the cells, *Cannarella et. al.* highlighted reduced SEI growth when 7 psi pressure was applied. Similar results were obtained in the present study, as shown in Figure 5. Both 5 and 15 psi conditions showed less capacity fade than the case where no additional pressure was applied, which is likely to be due to lower SEI growth. The exact mechanism leading to lower SEI formation when cells are under pressure is currently unknown and beyond the scope of this work, and will be studied in a future study. However, it can be concluded that, applying pressure, up to 15 psi can reduce the capacity fade of the battery; although a future study with a higher number of pressure points will be able to capture this characteristic and identify the optimum pressure to minimise capacity fade.

3.4.2 Impedance raise with cycling at different pressure

In contrast, applied pressure led to the increase of the pure Ohmic resistance of the battery, which has not been reported by any previous published work. Change of resistance is due to change of porosity and tortuosity of the separator and change of wettability of the electrodes. When pressure is applied, the resistance attributed to the ion transport resistance between electrodes through the separator increases (Eq. 1). Simultaneously, the wettability of the electrodes increases. That is, the penetration of the electrolyte deep into the porous electrodes increases. Increased wettability leads to better contact between electrode materials and electrolyte, leading to a reduction in the pure Ohmic resistance. With the presence of these two opposing mechanisms, pure Ohmic resistance R_o under a 5 psi and 15psi compressive pressure was found to increase.

Separator creep occurs even when small pressures are applied, however, the phenomenon is not linear with pressure [23]. For the cells considered in this study, the change of separator

creep and thus ion transport resistance at 15 psi compared to 5 psi may not be significant. However, the lower R_o increase at 15 psi compared to 5 psi may be due to the fact that wettability of the electrode has increased more at 15 psi than 5psi.

When wettability increases, the double layer area increases, which in-turn increases the double layer capacitance and reduces ion-transport resistance [29]. The smaller semicircle on the Nyquist plot after applying pressure, as shown in Figure 4, suggests better wettability of the electrodes.

When the cells are cycled, especially in a higher SoC window, gas forms due to side reactions [19, 30]. The pressure rise presented in Table 3 can also, in part, be due to gas formation. Due to the increased pressure with cycling, wettability of the electrodes increases, which, may have compensated for the degradation of double layer capacitance and charge transfer resistance. Therefore, the semicircle on the Nyquist plot remained unchanged with cycling as shown in Figure 6 (b) and (c). Furthermore, pure Ohmic resistance increased with the increase of separator creep which itself increased with pressure over cycling. The observed higher increase of pure Ohmic resistance at 5 psi condition compared to 15 psi condition with cycling requires further investigation with higher number of applied pressure conditions.

Although discussion on degradation mechanisms have been presented, to conclusively assign the observed capacity and power fade to particular mechanisms of degradation requires invasive testing, typically either *in situ* or post mortem. At present, there are no known *in situ* measurement techniques which can measure electrochemical mechanisms while cell is being electrically cycled under pressure. Therefore, the evolution of wettability and separator creep cannot be measured directly, rather estimates can only be inferred via heuristic models from cell parameters such as voltage, capacitance, resistance measured during the test.

4. Conclusion

Six 15 Ah $LiNiMnCoO_2$ and Graphite electrode pouch cells were cycled 1200 times under compressive pressure loads akin to pressure loads existing in automotive packs. Cells were subjected to either, atmospheric, +5psi or +15 psi compressive loads and subsequently cycled with a constant 1C charge and discharge rate between 100% and 50% SoC. Following every 150 charge/discharge cycles, the cells were characterised for degradation using a 1C capacity

test, pulse power tests and electrochemical impedance spectroscopy (EIS) tests at 90 %, 50 % and 20 % SoC.

In agreement with previous studies, we find that capacity fade reduced by 2.2 % and 2.4 % with the application of 5 psi and 15 psi compressive loads respectively. Unlike previous studies, however, this paper also considered the effect of compressive loads on power fade. The pulse power results show that at every timescale the resistance rise was lowest for atmospheric pressure and highest for 5psi. The average resistance rise (averaged across time scales) was 7.5 %, 39 % and 18 % respectively for 0 psi, 5 psi and 15 psi conditions. This contrast with the capacity fade results. From analysis of the origin of resistance, using EIS, it was found that the pure Ohmic resistance, associated with ion transport resistance of the separator, mainly contributes to this resistance rise. It was also found that, due to a contrasting mechanism, increased pressure with cycling improved the wettability and thus increased the double layer capacitance and reduced ion transfer resistance – which compensates, to some extent, the degradation of double layer due to cycling. This increase of resistance which contrast with capacity fade results, must be carefully considered by engineers in their respected fields of application. This study can contribute to determining the optimal external pressure for a particular cell type and application.

Acknowledgement

The research presented within this paper is supported by the Innovate UK (https://hvm.catapult.org.uk/hvm-centres/wmg-catapult/) through the WMG centre High Value Manufacturing (HVM) Catapult in collaboration with Jaguar Land Rover and TATA Motors. The authors are thankful to all 'cell work-stream' members of HVM Catapult for their valuable advice, comments and discussions.

Reference

1. Lee, J.H., H.M. Lee, and S. Ahn, *Battery dimensional changes occurring during charge/discharge cycles—thin rectangular lithium ion and polymer cells.* Journal of Power Sources, 2003. **119-121**: p. 833-837.
2. Kizilel, R., R. Sabbah, J.R. Selman, and S. Al-Hallaj, *An alternative cooling system to enhance the safety of Li-ion battery packs.* Journal of Power Sources, 2009. **194**(2): p. 1105-1112.

3. Hunt, I.A., Y. Zhao, Y. Patel, and J. Offer, *Surface Cooling Causes Accelerated Degradation Compared to Tab Cooling for Lithium-Ion Pouch Cells.* Journal of The Electrochemical Society, 2016. **163**(9): p. A1846-A1852.
4. Uddin, K., A. Picarelli, C. Lyness, N. Taylor, and J. Marco, *An Acausal electro-thermal Li-ion battery models for automotive applications.* Energies, 2014. **7**(9): p. 5675-5700.
5. Troxler, Y., B. Wu, M. Marinescu, V. Yufit, Y. Patel, A.J. Marquis, N.P. Brandon, and G.J. Offer, *The effect of thermal gradients on the performance of lithium-ion batteries.* Journal of Power Sources, 2014. **247**: p. 1018-1025.
6. Finegan, D.P., M. Scheel, J.B. Robinson, B. Tjaden, I. Hunt, T.J. Mason, J. Millichamp, M. Di Michiel, G.J. Offer, G. Hinds, D.J. Brett, and P.R. Shearing, *In-operando high-speed tomography of lithium-ion batteries during thermal runaway.* Nat Commun, 2015. **6**: p. 6924.
7. Sabbah, R., R. Kizilel, J.R. Selman, and S. Al-Hallaj, *Active (air-cooled) vs. passive (phase change material) thermal management of high power lithium-ion packs: Limitation of temperature rise and uniformity of temperature distribution.* Journal of Power Sources, 2008. **182**(2): p. 630-638.
8. Al-Hallaj, S. and J.R. Selman, *Thermal modeling of secondary lithium batteries for electric vehicle/hybrid electric vehicle applications.* Journal of Power Sources, 2002. **110**(2): p. 341-348.
9. Alhanouti, M., M. Gießler, T. Blank, and F. Gauterin, *New Electro-Thermal Battery Pack Model of an Electric Vehicle*. Energies, 2016. **9**(7): p. 563.
10. Mi, C., B. Li, D. Buck, and N. Ota. *Advanced Electro-Thermal Modeling of Lithium-Ion Battery System for Hybrid Electric Vehicle Applications*. in *2007 IEEE Vehicle Power and Propulsion Conference*. 2007.
11. Gao, Z., C. Chin, W. Woo, and J. Jia, *Integrated Equivalent Circuit and Thermal Model for Simulation of Temperature-Dependent LiFePO4 Battery in Actual Embedded Application.* Energies, 2017. **10**(1): p. 85.
12. Karimi, G. and X. Li, *Thermal management of lithium-ion batteries for electric vehicles.* International Journal of Energy Research, 2013. **37**(1): p. 13-24.
13. Mills, A. and S. Al-Hallaj, *Simulation of passive thermal management system for lithium-ion battery packs.* Journal of Power Sources, 2005. **141**(2): p. 307-315.

14. Khateeb, S.A., M.M. Farid, J.R. Selman, and S. Al-Hallaj, *Design and simulation of a lithium-ion battery with a phase change material thermal management system for an electric scooter*. Journal of Power Sources, 2004. **128**(2): p. 292-307.
15. Ryu, J.H., J.W. Kim, Y.-E. Sung, and S.M. Oh, *Failure Modes of Silicon Powder Negative Electrode in Lithium Secondary Batteries.* Electrochemical and Solid-State Letters, 2004. **7**(10): p. A306.
16. Verbrugge, M.W. and Y.-T. Cheng, *Stress and Strain-Energy Distributions within Diffusion-Controlled Insertion-Electrode Particles Subjected to Periodic Potential Excitations.* Journal of The Electrochemical Society, 2009. **156**(11): p. A927-A937.
17. Fu, R., M. Xiao, and S.-Y. Choe, *Modeling, validation and analysis of mechanical stress generation and dimension changes of a pouch type high power Li-ion battery.* Journal of Power Sources, 2013. **224**: p. 211-224.
18. Uddin, K., S. Perera, W. Widanage, L. Somerville, and J. Marco, *Characterising Lithium-Ion Battery Degradation through the Identification and Tracking of Electrochemical Battery Model Parameters.* Batteries, 2016. **2**(2): p. 13.
19. Vetter, J., P. Novák, M.R. Wagner, C. Veit, K.C. Möller, J.O. Besenhard, M. Winter, M. Wohlfahrt-Mehrens, C. Vogler, and A. Hammouche, *Ageing mechanisms in lithium-ion batteries.* Journal of Power Sources, 2005. **147**(1–2): p. 269-281.
20. Wang, X., Y. Sone, G. Segami, H. Naito, C. Yamada, and K. Kibe, *Understanding Volume Change in Lithium-Ion Cells during Charging and Discharging Using In Situ Measurements.* Journal of The Electrochemical Society, 2007. **154**(1): p. A14-A21.
21. Wang, X., Y. Sone, and S. Kuwajima, *In Situ Investigation of the Volume Change in Li-ion Cell with Charging and Discharging: Satellite Power Applications*. Journal of The Electrochemical Society, 2004. **151**(2): p. A273-A280.
22. Cannarella, J. and C.B. Arnold, *Stress evolution and capacity fade in constrained lithium-ion pouch cells.* Journal of Power Sources, 2014. **245**(0): p. 745-751.
23. Peabody, C. and C.B. Arnold, *The role of mechanically induced separator creep in lithium-ion battery capacity fade.* Journal of Power Sources, 2011. **196**(19): p. 8147-8153.
24. Cannarella, J. and C.B. Arnold, *Ion transport restriction in mechanically strained separator membranes.* Journal of Power Sources, 2013. **226**(0): p. 149-155.
25. Gering, K.L., *Diagnostic Testing and Analysis Toward Understanding Aging Mechanisms and Related Path Dependence*. 2012: DOE Vehicle Technologies Program Annual Merit Review.

26. Barai, A., G.H. Chouchelamane, Y. Guo, A. McGordon, and P. Jennings, *A study on the impact of lithium-ion cell relaxation on electrochemical impedance spectroscopy.* Journal of Power Sources, 2015. **280**(0): p. 74-80.
27. Gomez, J., R. Nelson, E.E. Kalu, M.H. Weatherspoon, and J.P. Zheng, *Equivalent circuit model parameters of a high-power Li-ion battery: Thermal and state of charge effects.* Journal of Power Sources, 2011. **196**(10): p. 4826-4831.
28. Marcinek, M., J. Syzdek, M. Marczewski, M. Piszcz, L. Niedzicki, M. Kalita, A. Plewa-Marczewska, A. Bitner, P. Wieczorek, T. Trzeciak, M. Kasprzyk, P.Łężak, Z. Zukowska, A. Zalewska, and W. Wieczorek, *Electrolytes for Li-ion transport – Review.* Solid State Ionics, 2015. **276**: p. 107-126.
29. Wu, M.-S., T.-L. Liao, Y.-Y. Wang, and C.-C. Wan, *Assessment of the Wettability of Porous Electrodes for Lithium-Ion Batteries.* Journal of Applied Electrochemistry, 2004. **34**(8): p. 797-805.
30. Broussely, M., P. Biensan, F. Bonhomme, P. Blanchard, S. Herreyre, K. Nechev, and R.J. Staniewicz, *Main aging mechanisms in Li ion batteries.* Journal of Power Sources, 2005. **146**(1–2): p. 90-96.
31. Sethuraman, V.A., M.J. Chon, M. Shimshak, V. Srinivasan, and P.R. Guduru, *In situ measurements of stress evolution in silicon thin films during electrochemical lithiation and delithiation.* Journal of Power Sources, 2010. **195**(15): p. 5062-5066.
32. Verma, P., P. Maire, and P. Novák, *A review of the features and analyses of the solid electrolyte interphase in Li-ion batteries.* Electrochimica Acta, 2010. **55**(22): p. 6332-6341.
33. Arora, P. and Z. Zhang, *Battery Separators.* Chemical Reviews, 2004. **104**(10): p. 4419-4462.